Journal of the European Ceramic Society 22 (2002) 2415–2425

www.elsevier.com/locate/jeurceramsoc

Texture, structure and chemistry of a boron nitride fibre studied by high resolution and analytical TEM

Fernand Chassagneux[a], Thierry Epicier[b,*], Pascaline Toutois[a], Philippe Miele[a], Christiane Vincent[a], Henri Vincent[a]

[a]*Laboratoire des Multimatériaux et Interfaces, umr CNRS 5615, Université Claude Bernard-Lyon1, 43 bd du 11 novembre 1918, F-69622 Villeurbanne Cedex, France*

[b]*GEMPPM, umr CNRS 5510, INSA de Lyon, Bât.502, F-69621 Villeurbanne Cedex, France*

Received 12 June 2001; received in revised form 27 November 2001; accepted 28 December 2001

Abstract

The present work is devoted to a TEM (transmission electron microscopy) study of the texture, structure and chemistry of a boron nitride (BN) fibre. The general structure of the fibre consists of two concentric parts; the near surface region is finely nano-crystallised, while the bulk of the fibre exhibits larger crystallites, although still of nanometric sizes. All grains appear to be randomly oriented with respect to the fibre axis, which makes the mechanical properties of this material remain modest. From a crystallographic point of view, both hexagonal and rhombohedral BN forms have clearly been identified by high resolution TEM (HRTEM). From a chemical point of view, EELS (electron energy loss spectroscopy) analysis shows that the N/B atomic ratio remains close to one, although it tends to decrease slightly from the outer surface to the 'core'. No significant amount of impurities (e.g. carbon and oxygen) has been detected. The study of the B–K and N–K edges reveals a great similarity between the hexagonal and the rhombohedral forms. © 2002 Published by Elsevier Science Ltd.

Keywords: BN; EELS; Electron microscopy; Fibres; BN fibres

1. Introduction

Boron nitride based materials possess a wide range of interesting chemical, mechanical and electrical properties. Boron nitride presents a better oxidation resistance compared to carbon, and can also be obtained under the form of micronic fibres;[1,2] indeed, the fibre of interest here has been elaborated via a chemical route involving a polymer as a precursor.[1]

The present work has been undertaken in the course of a general study of BN fibres, to be used for thermo-mechanical applications. According to the need for a fine microstructural characterization to understand the mechanical properties of the fibres, and optimise the elaboration conditions, it appears that TEM is a well-adapted tool: the high spatial resolution of the microscope allows the fibre to be probed through radial line-scans, and analytical accessories such as EELS allows the light elements B, N, C and O to be efficiently analysed. The combination of these performances is a great advantage to overcome some difficulties specific to boron nitride fibres, and especially the detection of carbon, which can be present within the material, but can also arise from different contamination sources.

As it will be shown hereafter, the fibre which has been studied here possesses an heterogeneous microstructure, which makes it interesting to collect detailed textural, structural and chemical information in order to optimise the elaboration process.

2. Experimental background

2.1. Preparation of fibres

The boron nitride fibres are elaborated through a chemical route described elsewhere[1] and summarized in Fig. 1. A precursor, Tri(methylamino)borazine (MAB), is heated to form a polymeric compound, which is extruded with a drawplate of 200 μm diameter. Final

* Corresponding author.
E-mail address: thiery.epicier@insa-lyon.fr (T. Epicier).

0955-2219/02/$ - see front matter © 2002 Published by Elsevier Science Ltd.
PII: S0955-2219(02)00002-X

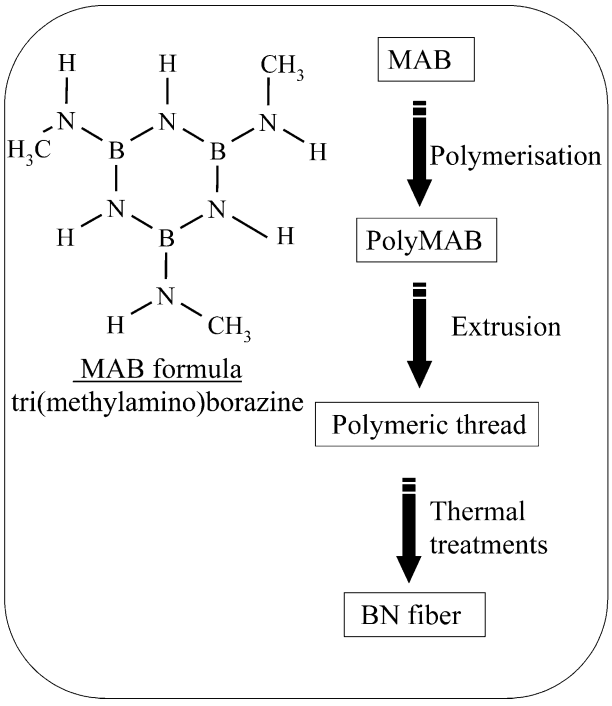

Fig. 1. Elaboration scheme of the BN fibres.

fibres are obtained by a further thermal treatment of these wires, up to 1800 °C under ammonia then nitrogen atmosphere.

2.2. Electron microscopy

After a general analysis by X-ray diffraction work, the fibre is observed in a scanning electron microscope then prepared for TEM observation, according to the procedure given below.

2.2.1. Thin foils preparation

Fragments of fibres of about 1 cm in length are aligned and embedded in an epoxy resin (EPON A), which is polymerized first at room temperature and finally at 50 °C.

After a rough slicing with a diamond saw, blocs of fibres are cut with an ultramicrotom equipped with a diamond knife (LEICA S). Several slabs of about 50 ± 20 nm in thickness are deposited on a carbon holey grid. Two types of cutting have been made, either perpendicular or parallel to the fibre axis. Although undesirable charging effects perturb the TEM observation, no further carbon coating was performed on the grids, evidently to make it possible to analyse the presence of 'intrinsic' carbon.

2.2.2. Microscopes

A 200 kV microscope, TOPCON EMB-002B, has been used for a general characterization of the fibres in both imaging and diffraction modes (diffraction patterns were obtained on 0.5 μm selected areas—SAD patterns).

A nano-characterization was performed on a field-emission gun microscope, Jeol 2010F. High resolution images were recorded numerically with the aid of a GATAN slow-scan CCD, in order to shorten exposure times and minimize the 'bougés' due to charging effects. The energy dispersive X-ray analyser (OXFORD Link-Isis, with an ultra-thin window allowing light elements down to boron to be detected) mounted on this instrument was occasionally used for chemical analysis of the fibre, but most analytical work was conducted in electron energy-loss spectroscopy (EELS) as summarized in the next sub-section.

2.3. EELS analysis

The Jeol 2010F machine used in this work, being equipped with a GATAN DigiPeels parallel spectrometer, an extensive EELS study has been performed in an energy-range 0–600 eV typically (i.e. from the elastic peak and low-loss features, to the boron, carbon, nitrogen and oxygen K-edges near respectively 188, 294, 400 and 532 eV). Those spectra were classically corrected from the gain variations of the detector, and a quantitative analysis of the chemical composition was performed with the GATAN EL/P program after a usual Fourier-ratio deconvolution of the plasmon peaks (see [3] for further details concerning EELS work). Most of the spectra were acquired during short times (from 0.2 to 4 s), from single nano-crystallites, using probe sizes from 0.4 to about 4 nm; under those conditions, the energy-resolution, measured as the full-width at half-maximum of the zero-loss peak, was 1 ± 0.1 eV, and the convergence and collection half-angles were respectively about 8 and 4 mrad.

3. Results

3.1. General microstructure

Fig. 2 is a typical SEM micrograph of a broken fibre, about 40 μm in diameter, showing its internal structure. It is seen that the central region of the fibre, with a diameter of about 35 μm, has a granuleous aspect, while the periphery of the fibre consists in an apparently homogeneous layer of about 2 μm in thickness. The presence of a micro-crack between these two parts probably reveals the existence of thermal stresses.

TEM, low-magnification, micrographs confirm this organization; Fig. 3 shows a longitudinal section (knife plane parallel to the fibre axis), where a relatively well-crystallized region is seen in the centre part of the fibre, while the outer region consists in finer nano-crystallites. Selected-area diffraction, 'Debye-Scherrer'-type, patterns shown in Fig. 3 clearly point out the difference between these two regions, which will be labelled

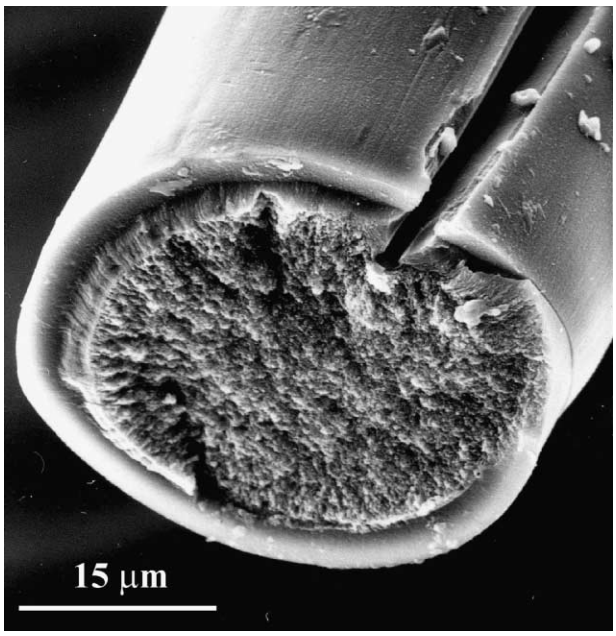

Fig. 2. SEM view showing the general microstructure of a fractured fibre.

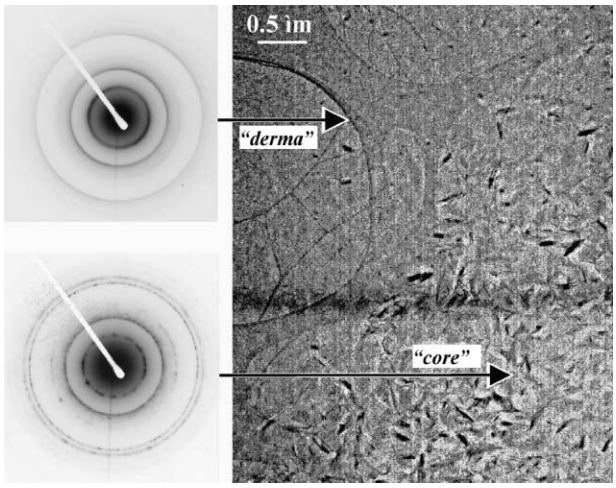

Fig. 3. TEM micrograph of a longitudinal section and diffraction patterns of the "derma" and "core" regions as indicated.

'core' and 'derma' respectively in the following: diffraction rings from the 'core' are finer and exhibit more discrete spots than that of the 'derma', which proves that the mean crystallite size is larger in the 'core'. Both patterns can consistently be indexed as hexagonal BN,[1] but this point will be re-examined later.

The same heterogeneity is observed in transverse sections (knife plane perpendicular to the fibre axis), as shown by Fig. 4.

[1] Hexagonal BN belongs to the space group P63/mmc (No.194), with $a = 0.25044$ and $c = 0.66562$ nm (JCPDS file 34 421); B and N atomic species are respectively located in (2d) and (2c) Wyckoff positions.

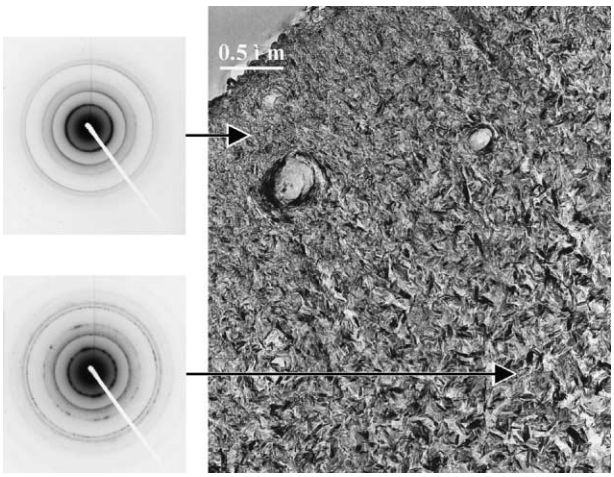

Fig. 4. TEM micrograph of a transversal section and diffraction patterns of the "derma" and "core" regions as indicated.

According to the fact that all SAD patterns exhibit continuous diffraction rings, without noticeable absence of any $\{hkl\}$ reflections, it can be concluded that the crystallographic orientations of the particles in both 'core' and 'derma' regions are randomly distributed (it is well-known that preferential, or textural, orientations are revealed by discontinuities or absence of rings in 'Debye-Scherrer'-type electron diffraction patterns, especially in the case of fibre-type textures).

The presence of internal pores, generally located under the 'derma' region and up to 0.5 μm in diameter is clearly evidenced in the transverse section (Fig. 4).

A conventional TEM work [i.e. a combination of bright and dark field imaging with the $(0002)_{BN}$ reflection] allows the dimensions of the crystallites to be estimated. From micrographs such as those reported in Fig. 5, the characteristic lengths $L_{//}$ and $L_{\perp}$, respectively parallel and perpendicular to the c-axis of the hexagonal BN cell, can be measured. Average values are reported in Table 1; although a large scatter of about 20% has been observed on several dozens of particles, these results re-emphasize the difference between the 'core' and the 'derma': 'core' crystallites are more elongated (aspect ratio $L_{//}/L_{\perp} \approx 3.6$) than those from the 'derma', which are moreover clearly smaller.

3.2. High resolution imaging

3.2.1. General overview

HRTEM multi-beam images are dominated by the apparition of basal $(0002)_{BN}$ lattice fringes, easily resolved at ≈ 0.33 nm in all crystallites oriented with their c-axis roughly perpendicular to the incident beam direction. In the very near surface region (i.e. over a distance of a few nanometers in the outer part of the 'derma', see Fig. 6), those planes run parallel to the fibre surface, and appear to be more continuous than anywhere else within the 'derma'. The same observation

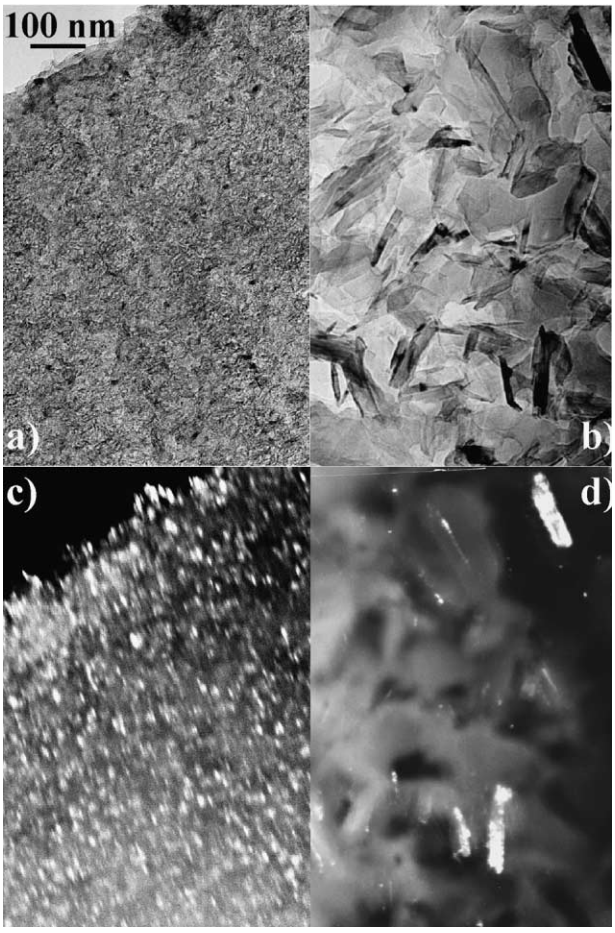

Fig. 5. TEM bright field images (a and b) of the ''derma'' and ''core'' regions (a) and (b), respectively and associated dark field images (c) and (d), respectively.

Table 1
Crystallites sizes $L_{//}$ and $L_{\perp}$

	''Derma''		''Core''	
	$L_{//}$ (nm)	$L_{\perp}$ (nm)	$L_{//}$ (nm)	$L_{\perp}$ (nm)
Longitudinal section	5	5	25	100
Transversal section	5	5	25	80

Table 2
N/B atomic ratio (deduced from EELS analyses) in relation with the probe position r (distance from the fibre edge)

Distance from the fibre edge r (μm)	<0.1	0.3	0.7	2	5
N/B atomic ratio	1.10± 0.14	1.00± 0.16	0.99± 0.16	0.91± 0.15	0.98± 0.16

can be made at the very close vicinity of internal pores, such as in Fig. 7.

Further representative lattice images are reported in Fig. 8. In Fig. 8(a), bended (0002) fringes are observed; the 'finger-print' aspect of such images is not as pronounced as in the case of graphitic carbon fibres, mainly

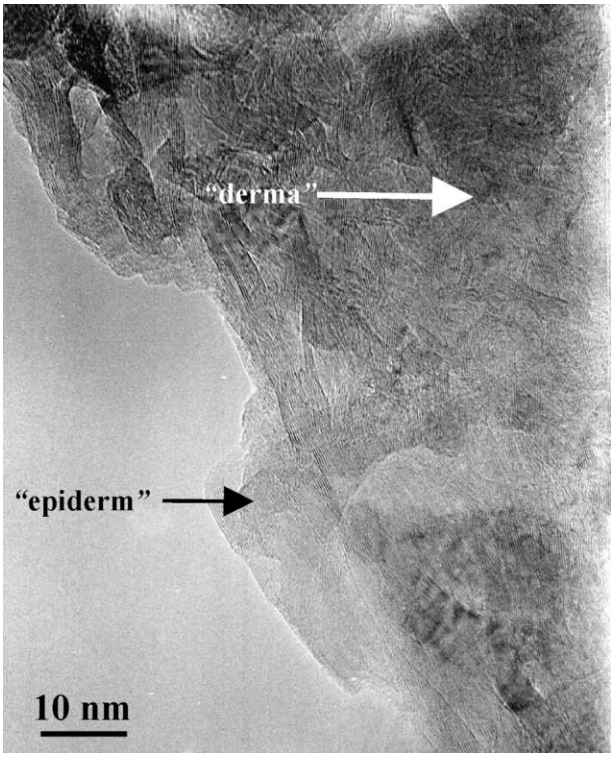

Fig. 6. TEM view showing the fibre edge.

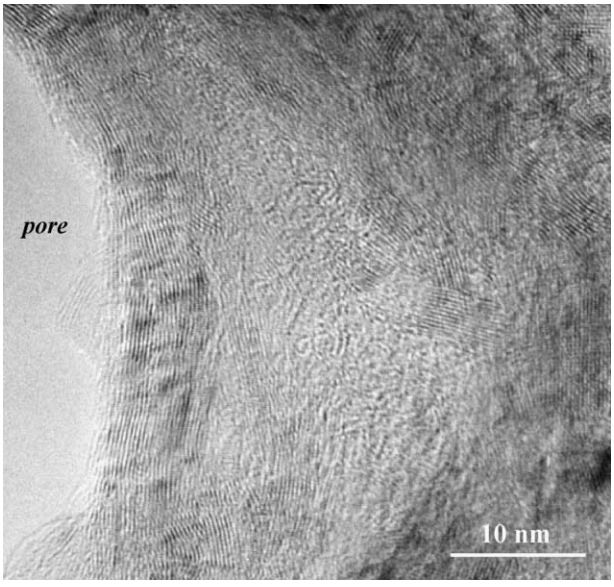

Fig. 7. HRTEM view showing a pore edge.

because the crystallites here are very small, and owing to the larger rigidity of BN compared to that of graphite.[4] Fig. 8b is a micrograph from the 'core'. Elongated crystallites occasionally exhibit wavy basal fringes, and significant curvatures or bendings, generally near 130°. Well-defined Moirés patterns are frequently observed, owing to the superposition of several crystallites; the homogeneity of these Moirés patterns indicates that few lattice defects exist within the particles.[5]

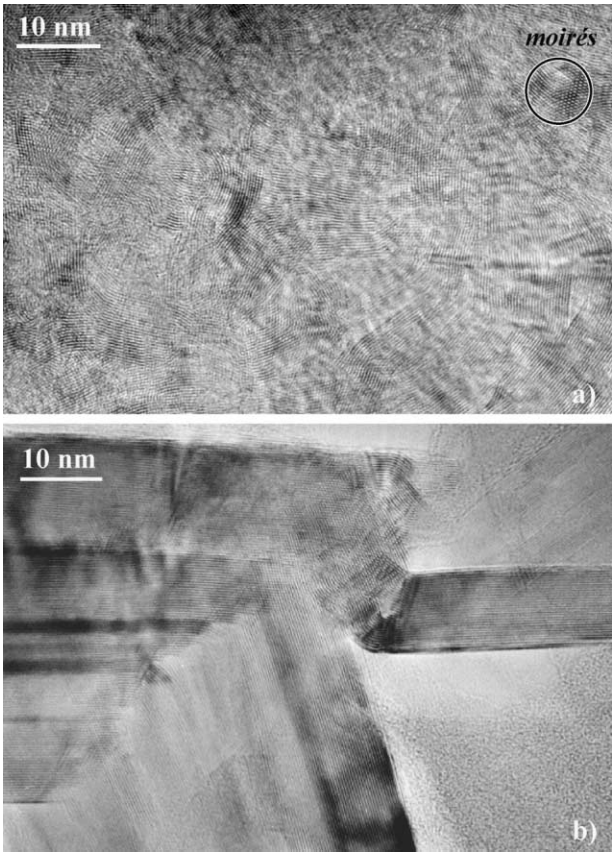

Fig. 8. Lattice images of a longitudinal section: (a) "derma", (b) "core".

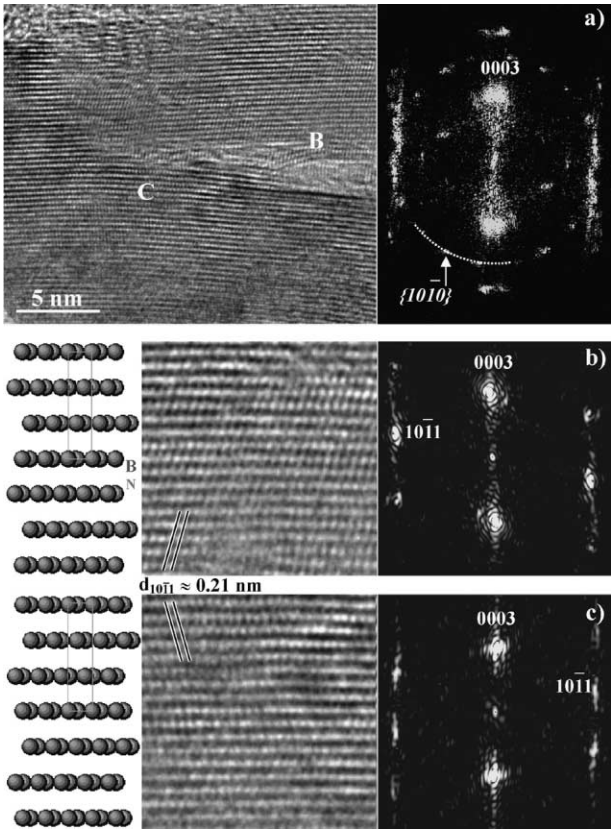

Fig. 9. HRTEM imaging of rhombohedral BN; (a): micrograph showing a particle made of 2 rhombohedral crystals roughly in a twinned orientation and viewed perpendicularly to their *c*-axis; the associated diffractogram shows the evidence of the $\{10\text{–}10\}_{\text{hexagonal}}$ ring, arising from underlying nano-crystals; (b): enlargement of region labelled B in (a), and indexing of the $[1\text{–}210]_{\text{rhombohedral}}$ diffractogram; (c): same as (b) from region C.

Besides the crystalline areas where the basal planes are resolved, a very large proportion of the observed surface does not exhibit easily discernable lattice fringes (see Fig. 8b); from simple geometrical considerations, it can be expected than those regions are nano-crystallized, and do correspond to the superimposition of small particles with their c-axis more or less parallel to the electron beam. In fact, it must be reminded here that the mean size of the crystallites parallely to their *c*-axis ($L_{//}$ ≈25 nm in the 'core') remains small compared to the thickness of the ultramicrotomic sections (about 50 nm); then, such crystallites may easily superimpose when they are oriented with their c-axis parallel to the electron beam. This, plus the fact that turbostratic arrangements of domains sharing the same *c*-axis may exist within these particles, means that no lattice fringe can be resolved with a high contrast for those regions.

All these remarks have motivated a closer inspection of the crystallographic nature of the 'core', which is reported in the next sub-section.

3.2.2. *Crystallographic nature of the particles within the 'core'*

Numerous observations have been made in order to examine crystallites oriented along a low-index azimuth. Fig. 9 is a representative example of particles exhibiting another type of lattice fringes, in addition to the basal fringes at 0.33 nm.

The diffractograms obtained by numerical fast-fourier transfom (FFT) show reflections at about 0.210 nm [according to the internal calibration permitted by the (0002) reflection at 0.333 nm], which form an angle of $77 \pm 1^\circ$ with respect to the basal fringes. this value can be compared to inter-reticular distances and angles between $\{hkl\}$ planes as deduced from the JCPDS files for hexagonal and rhombohedral BN (respectively: files 34 421 and 45 1171):

hexagonal BN:	$d_{10\text{–}10} = 0.217$ nm, angle (0002,10–10) = 90° $d_{10\text{–}11} = 0.206$ nm, angle (0002,10–11) = 71.9°
rhombohedral BN:	$d_{0003} = 0.3334$ nm $d_{10\text{–}11} = 0.212$ nm, angle (0003,10–11) = 77.8°

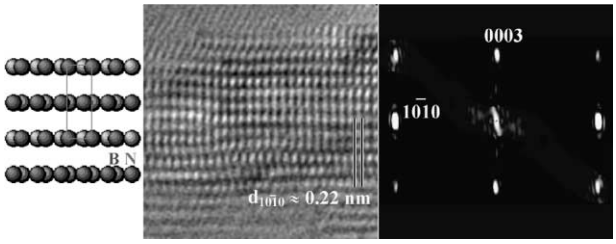

Fig. 10. HRTEM image [similar to Fig. 9(b) and (c)] of a particle of hexagonal BN viewed along the $[1\text{–}210]_{hexagonal}$ direction.

From[2] these data, it can be ascertained that the BN particle shown in Fig. 9 corresponds to the rhombohedral form, viewed along the [1–210] azimuth.

A similar analysis can be made on hexagonal BN particles viewed along the [1–210] azimuth, as illustrated by Fig. 10.

Both hexagonal and rhombohedral phases are then co-existing within the fibre; although no statistical analysis has been made on the crystallites oriented with their *c*-axis perpendicular to the electron beam direction (i.e. those exhibiting basal lattice fringes), it appears that at least 50% of such particles are of the rhombohedral type.

The examination of crystallites having their **c**-axis parallel, or roughly parallel to the incident beam direction is more puzzling: firstly, it must be emphasized that HRTEM imaging of rhombohedral crystals along the [0001] direction is not easy, since the first visible reflections in this azimuth, i.e. the {11–20} planes have an inter-reticular distance equal to 0.125 nm, which is very difficult to resolve, even with a 'FEG' microscope; secondly, the superimposition problem evoked in Section 3.2.1 does not help isolated and homogeneous crystallites to be imaged unambiguously. It has, however, been possible to obtain reasonably good [0001] images of such isolated hexagonal crystals, as is shown in Fig. 11.

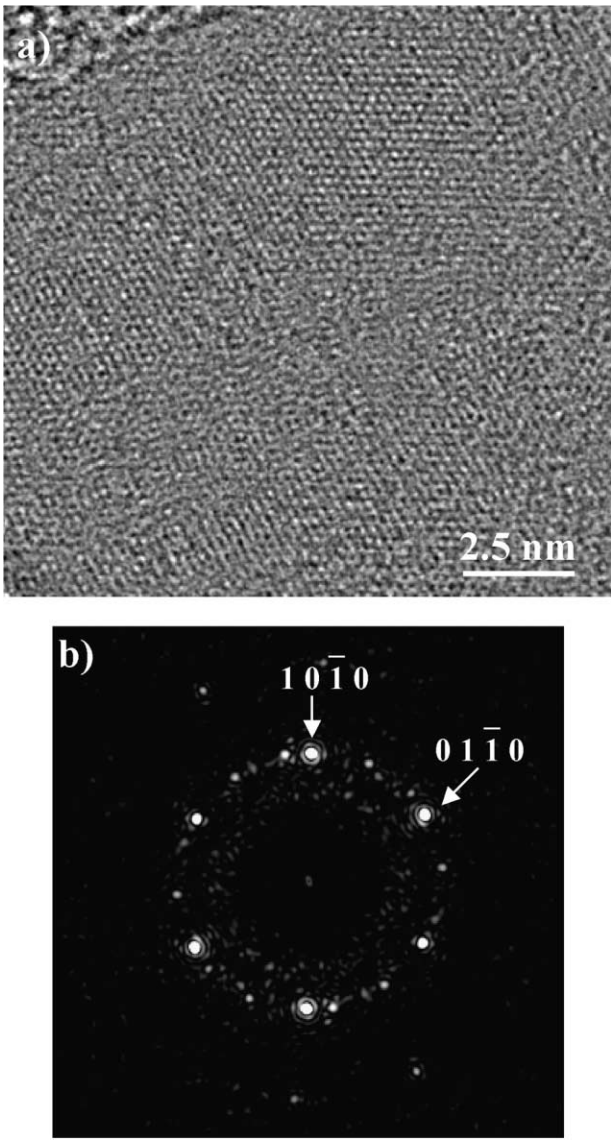

Fig. 11. HRTEM image and FFT of a "gangue" region, where a nanodomain of hexagonal BN is viewed along the *c*-axis.

3.3. EELS analysis

One of the great interests of the 2010F microscope used in the present study is that it allows HRTEM images and nano- or sub-nano probe EELS spectra to be obtained simultaneously on the same areas. As an example, the EELS spectra corresponding to the particles respectively shown in Figs. 10 and 11 are reported in Fig. 12.

The fine structure of the B–K and N–K edges presents the classical features that have been reported for hexagonal BN,[6] or BN compounds involving sp2 bonding.[7,8] Each of these edges (for example, the B–K edge near 188 eV) shows a first sharp pre-peak due to the $1s \rightarrow \pi*$ transition, followed by a second one, due to the $1s \rightarrow \sigma*$ transition; these peaks are respectively labeled $\pi*$ and $\sigma*$ in Fig. 12, and are common to the N–K edge near 401 eV. The ratio between these $\pi*$ and $\sigma*$ peaks is affected by a well-known anisotropic effect, regarding the orientation of the *c*-axis of 'graphitic'-type structures with respect to the incident beam direction:[9] owing to the large collection angle in the nano-probe mode, the pre-peak $\pi*$ is enhanced in the perpendicular orientation (see Fig. 12).

From Fig. 12, it is clear that very few, if any, carbon or oxygen pollution can be confidently detected (the atomic content for these two elements remains nominally lower than a few % in all spectra recorded in conditions similar to that shown in Fig. 12).

[2] Rhombohedral BN belongs to the space group R3m (No.160), with $a = 0.2504$ and $c = 1.000$ nm (JCPDS file 45 1171); B and N atomic species are located in (3a) Wyckoff positions, with z respectively equal to 0 and 0.3333.

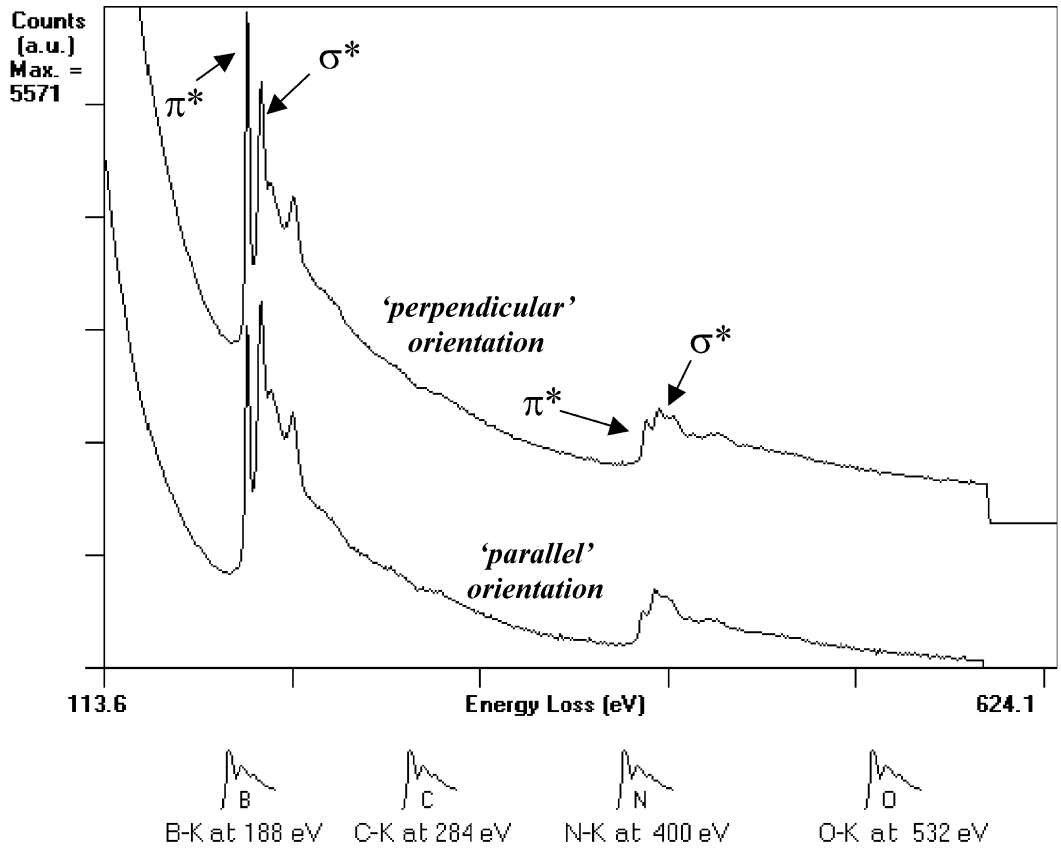

Fig. 12. PEELS spectra from the hexagonal BN particles shown in Figs. 10 and 11.

The presence of carbon in the analysed area has, however, clearly been observed occasionally, in regions where a superficial contamination by the embedding resin has occurred during the ultramicrotomic cutting; a typical example is shown in Fig. 13 where 3 spectra are shown. The first one (labelled 1) is from a rhombohedral particle where no significant amount of carbon is present; the second one (labelled 2) shows a region where the C–K edge is clearly present; this spectrum comes from a crystallite oriented with its *c*-axis roughly parallel to the electron beam. The third spectrum (3) is a representative one from an hexagonal particle within a fibre debris deposited on a holey carbon grid without any resin: it shows the cleanness of the BN material regarding carbon (more than 20 such debris have been analysed in the same way). It is worth noting the similarity of the B–K and N–K fine structures in spectra 1 and 3, which correspond respectively to the rhombohedral and hexagonal forms of BN.

About 50 spectra have been recorded from 2 nm regions in order to establish the atomic N/B ratio as a function of the radial distance *r* to the external surface of the fibre (see Table 2); at each position *r*, the results were averaged from that obtained from the same number of crystallites viewed with the incident beam either perpendicular or parallel to their *c*-axis orientations (as in Figs. 10 and 11, respectively), in order to minimize the possible influence of the anistropic effect previously mentioned[9] on the chemical analysis. Typical examples of analysed spectra are shown in Fig. 14.

4. Discussion

The TEM study of the general microstructure of the BN fibre of interest has pointed out its heterogeneity, mainly in terms of a different crystallite size between the outer and inner parts of the fibre ('derma' and 'core' regions respectively). The results obtained concerning the chemical composition of these BN particles as a function of the radial distance seem to indicate a slight nitrogen enrichment near the surface, which is probably due to the exit flux of nitrogen-rich gases produced during the high temperature processes. This can also be correlated to the size difference: it can then be stated that the smaller crystallite size at the periphery of the fibre ('derma' region) is the result of an incomplete ceramisation step, which is made more difficult owing to the perturbation created by the gas flux. Further work is in progress on other different fibres, in order to check if the crystallite size can also be directly correlated to the N/B ratio.

However, the N/B ratio remains close to one, which is consistent with previous XPS (X-ray photoelectron

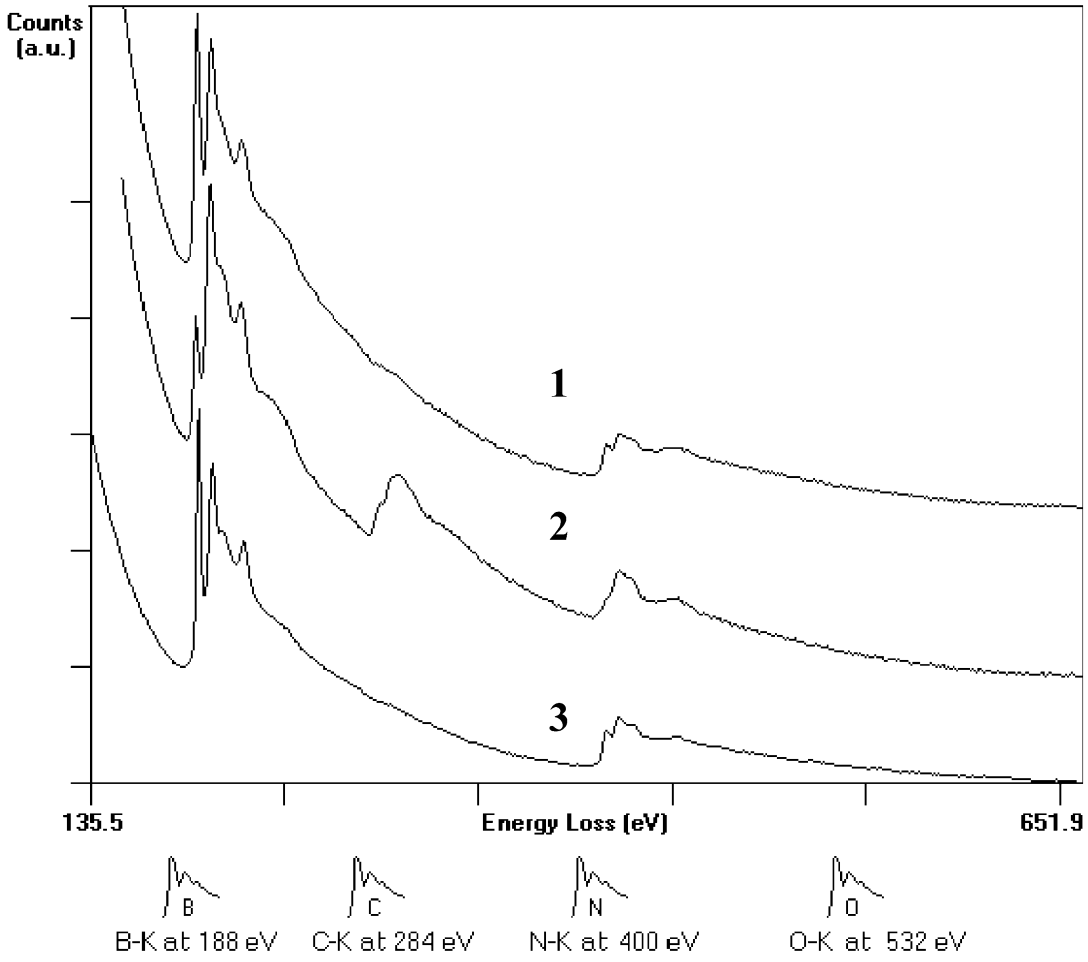

Fig. 13. PEELS spectra from various BN particles; from top to bottom: 1: rhombohedral crystallite in an ultramicrotomic section; 2: other crystallite in the same sample, showing the occasional presence of carbon ("gangue" region); 3: hexagonal crystallite in a fibre debris deposited onto a holey carbon grid.

spectroscopy) measurements performed on very similar fibres;[10] no other chemical difference was evidenced, especially as a function of the radial distance, concerning the very minor contents of carbon and oxygen impurities.

Concerning the texture of the fibre, no difference occurs regarding the orientation of the particles, which appears to be randomly distributed in any position within the fibre. It is known that the absence of any pronounced texture does not optimise the mechanical properties of ex PAN Carbon[11] or BN[2] fibres; this could explain the relatively modest fracture stress measured in the present case, that is 400 MPa, compared to 1200 MPa in the case of textured fibres.[12] These mechanical performances are certainly also degraded by the presence of internal pores in a sub-surface region.

The co-existence of both hexagonal and rhombohedral forms of boron nitride has clearly been evidenced by HRTEM. The rhombohedral phase was initially obtained by a chemical reaction between molten boric acid and potassium cyanide;[13] it was further shown that heating turbostratic and badly crystallized BN between 750 and 900 °C in the presence of halogen, or, more efficiently, alkaline cyanide, promotes the formation of rhombohedral BN.[14] The rhombohedral phase has also recently been evidenced in BN nano-tubes.[15] In the present case, it is believed that during the heat treatment of the wired precursor, ammonium cyanide may form, which then promotes the formation of the rhombohedral phase near 1000 °C, when BN crystallizes. Although no statistics were established from the HRTEM work, both hexagonal and rhombohedral forms seem to occur equiprobably and in any position within the fibre. It must be emphasized that electron diffraction does not allow us to discern, and a posteriori quantify properly the hexagonal and rhombohedral phases (see Fig. 15 and Table 3). Considering the smallness of the crystallites present in the fibre, X-ray diffraction does only bring support to the hypothesis of a turbostratic-type structure. Indeed, HRTEM imaging confirms this finding: (i) it is difficult to produce a sharp contrast of atomic columns within crystallites in the 'parallel' orientation, as expected in the case of a turbostratic-like

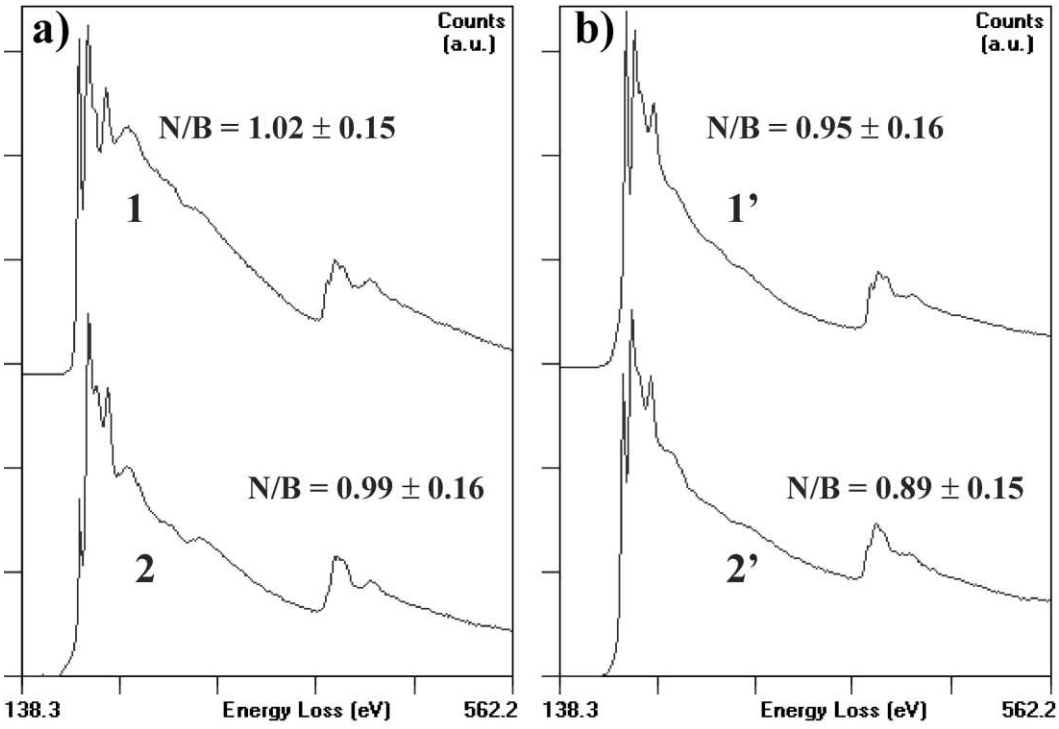

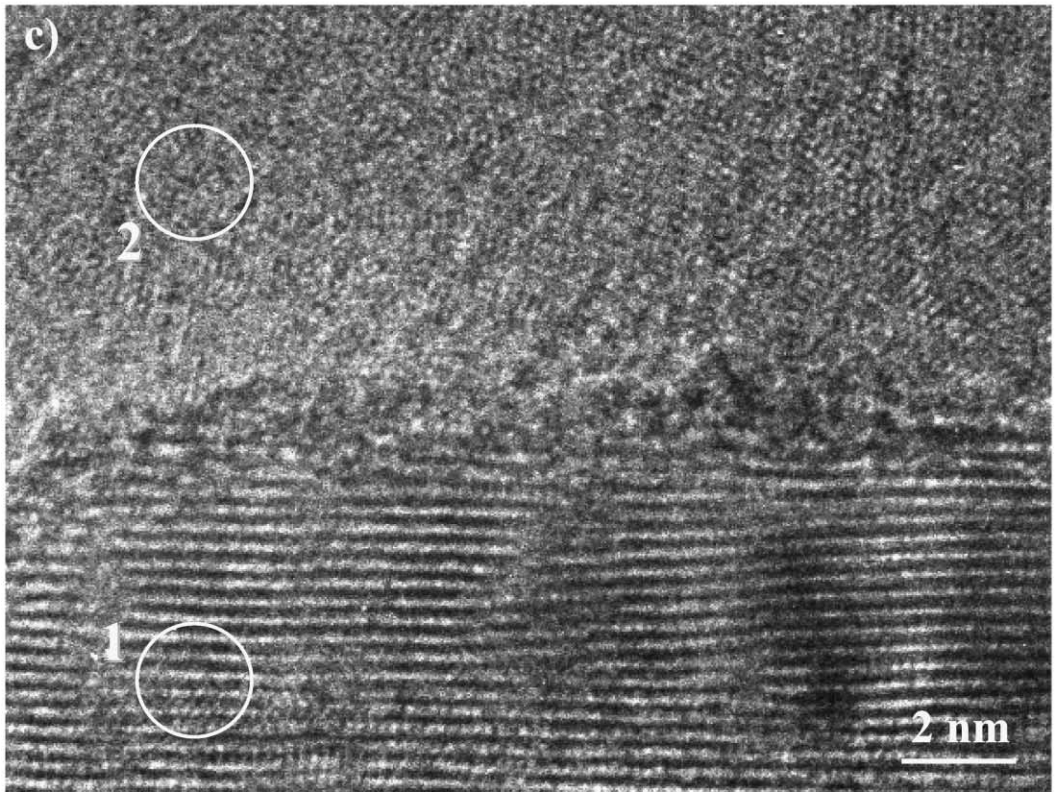

Fig. 14. EELS determination of the atomic N/B ratio; (a): analysis of 2 close regions, at about 0.7 μm from the fibre edge, and shown in (c) (probe size 2 nm) in 'perpendicular' and 'parallel' orientations (1 and 2 respectively); (b): same as (a) for 2 other close regions 1′ and 2′ at 2 μm from the fibre edge; (c): HRTEM image showing the crystallites analysed in (a).

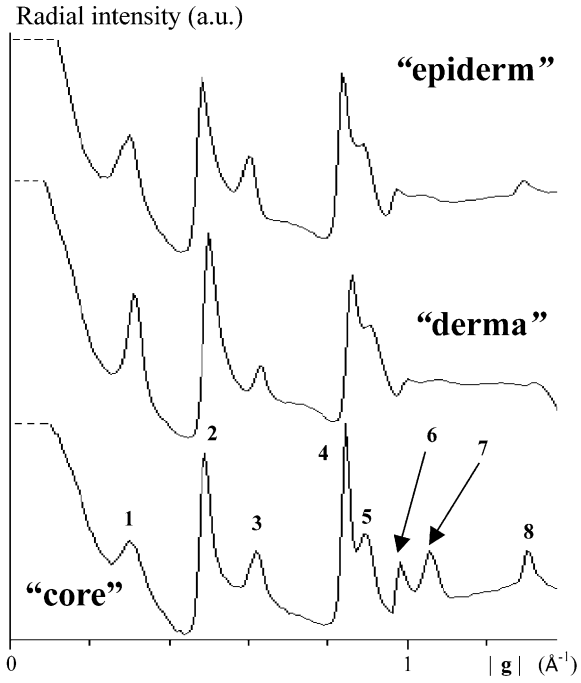

Fig. 15. Electronic diffraction pattern profile of turbostratic BN.

Table 3
Indexing of diffraction patterns in the hexagonal and rhombohedral phases of BN

Line number	Measured d (Å)	$(hkl)_{Hex}$ d (Å)	$(hkl)_{Rh}$ d (Å)
1	3.33	002	003
		3.281	3.334
2	2.11	100–101	101
		2.1693–2.0619	2.1196
3	1.67	004	006
		1.6636	1.66
4	1.24	110	110
		1.2521	1.2518
5	1.18	112	113
		1.172	1.1727
6	1.074	200	202
		1.0843	1.0599
7	1.005	114	116
		1.0005	1.001
8	0.8225	116	119
		0.8304	0.8312

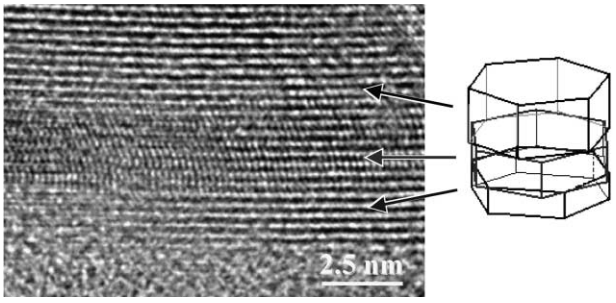

Fig. 16. HRTEM evidence of the intercalation of disoriented BN slabs but sharing the same c-axis, as schematically represented on the right-hand side.

arrangement; (ii) direct HRTEM evidence of the intercalation of nanometric slabs with parallel basal planes, but different in-plane orientations, has frequently been obtained within crystallites in the 'perpendicular' orientation (see Fig. 16).

5. Conclusion

The improvement of mechanical properties of BN fibres requires a good knowledge of the crystallisation processes, and a correlated optimisation of the texture; both aspects have been studied by means of TEM.

For the fibre of interest, the poor mechanical resistance is clearly attributed to the absence of any preferential orientation of the nano-sized BN crystallites, and also possibly to the presence of pores in a sub-surface region.

The general microstructure of the fibre has been shown to consist of an outer region, a few micrometers thick, called the 'derma', and a central 'core' region. These 2 regions do not differ from a structural point of view: they both consist of an apparent equal distribution of hexagonal and rhombohedral BN phases. However, 'derma' crystallites are significantly smaller than 'core' ones, as evidenced by electron diffraction and direct TEM imaging. From a chemical point of view, both regions appear to be free of significant amounts of impurities (e.g. carbon and oxygen); it is, however, suggested that the external 'derma' layer exhibits a greater N/B ratio than the 'core', which could explain the smallest crystallite size in the former region.

Another interesting finding of this study is the coexistence of hexagonal and rhombohedral BN phases. As revealed by EELS, it appears that B–K and N–K edges within the rhombohedral form are very similar to those observed in the hexagonal form (see spectra 1 and 3 in Fig. 13). Similar features have recently been reported for the rhombohedral BN phase but identified in nano-tubes. This similarity indicates a similarity of the electronic structure of these 2 phases, which is somewhat surprising owing to their crystallographic differences. A further study of the low-loss region by EELS is in progress to detail this point.

Acknowledgements

Thanks are due to the CLYME (Consortium Lyonnais de Microscopie Electronique) for the access to the TEM–FEG microscope.

References

1. Magnani, G., Richard, C. and Trichon, R., *Procédé de Préparation de Polyaminoborazines*, French Patent, FR 2 695 645, 1992.

2. Okano, Y. and Yamashita, H., *Boron Nitride Fiber and Process for Production Thereof*, US Patent, US 5 780 154, 1998.
3. Egerton, R. F., *Electron Energy-Loss Spectroscopy in the Electron Microscope*. Plenum Press, New York, 1996 p. 485.
4. Bacon, R., Carbon fibers from rayon precursors. *Chemistry and Physics of Carbon*, 1973, **9**, 1–102.
5. Guigon, M. and Oberlin, A., Preliminary studies of mesophase-pitch-based carbon fibres: structure and microtexture. *Composites Science and Technology*, 1986, **25**, 231–241.
6. Goldberg, D., Bando, Y., Eremets, M., Takemura, K., Kurashima, K. and Yusa, H., Insights into the structure of BN nanotubes. *Appl. Phys. Lett*., 1996, **69**(14), 2045–2047.
7. Schmid, H. K., Phase identification in carbon and BN systems by EELS. *Microsc. Microanal. Microstruct*., 1995, **6**(1), 99–111.
8. Loiseau, A., Willaime, F., Demoncy, N., Hug, G. and Pascard, H., Boron Nitride nanotubes with reduced numbers of layers synthesized by arc discharge. *Physical Review Letters*, 1996, **76**(25), 4737–4740.
9. Leapman, R. D., Fejes, P. L. and Silcox, J., Oirentation dependance of core edges from anisotropic materials determined by inelastic scattering of fast electrons. *Phys. Rev. B*, 1983, **28**, 2361–2373.
10. Vincent C., unpublished results.
11. Bennett, S. C. and Johnson, D. J., Electron microscope studies of structural heterogeneity in PAN-based carbon fibers. *Carbon*, 1979, **l17**, 25–39.
12. Toutois P., Thesis, in progress.
13. Herold, A., Mareluf, B. and Perio, P., Préparation et structure du nitrure de bore. *C.R. Acad Sci. Paris*, 1958, **246**(I), 1866–1868.
14. Sato, T., An effective anion series for the catalysis of the formation of rhombohedral boron nitride (rBN), Proc. 11th Int. Symp., Boron, Borides and Related Compounds Tsukuba (JAPAN). *J.J.A.P. series*, 1994, **10**, 158–159.
15. Bourgeois, L., Bando, Y. and Sato, T., Tubes of rhombohedral boron nitride. *J. Phys. D: Appl. Phys*., 2000, **33**, 1902–1908.